Magnetic field angle dependence of the magnetic phase diagram in UNi_4B

Hiroyuki Hidaka[1],* Tatsuya Yanagisawa[1], Chihiro Tabata[2],
Fusako Kon[1], Hiroshi Amitsuka[1], Yusei Shimizu[3], and Dai Aoki[4]
[1] *Graduate School of Science, Hokkaido University, Sapporo, Hokkaido 060-0810, Japan*
[2] *Materials Sciences Research Center, Japan Atomic Energy Agency, Tokai, Ibaraki 319-1195, Japan*
[3] *Institute for Solid State Physics, The University of Tokyo, Kashiwa, Chiba 277-8581, Japan*
[4] *Institute for Materials Research, Tohoku University, Oarai, Ibaraki 311-1313, Japan*
(Dated: October 28, 2025)

A uranium-based metallic compound UNi_4B with an orthorhombic structure exhibits antiferromagnetic (AFM) ordering at $T_N = 20.4$ K. Although an electric current-induced magnetization below T_N has been observed in this compound [H. Saito et al., J. Phys. Soc. Jpn. **87**, 033702 (2018)], its underlying mechanism remains controversial. In this study, we measured thermal expansion and magnetostriction along the a axis under a magnetic field H up to 14 T applied within the bc plane to investigate the rotational symmetry of a magnetic field–temperature (H–T) phase diagram in UNi_4B. From the phase diagrams constructed under various H angles between b and c, it is suggested that the H–T phase diagram practically exhibits sixfold rotational symmetry within the bc plane despite an orthorhombic crystal structure, which would be attributed to a quasihexagonal structure formed by U ions with small orthorhombic distortion.

I. INTRODUCTION

Cross-correlation phenomena, such as magnetoelectric and magnetoelastic responses, have attracted considerable attention since the discovery of a magnetoelectric (ME) effect in an insulating antiferromagnet Cr_2O_3. [1, 2] Half a century has passed since that discovery, and this research field has made remarkable progress both theoretically and experimentally. According to recent theoretical studies [3–5], the concept of augmented multipoles, which are spatially extended multipoles, is a useful framework for understanding the cross-correlation phenomena. In addition, these theoretical studies pointed out the emergence of cross-correlation phenomena not only in insulating systems but also in metallic ones. For example, the emergence of current-induced magnetization (M), which is attributed to the ferroic ordering of a magnetic toroidal dipole (MTD), was first predicted theoretically [6] and later observed experimentally in a magnetic metal UNi_4B. [7] Such a current-induced cross-correlation response has also been reported in other magnetic metals, such as current-induced M in Ce_3PtBi_5 [8] and current-induced strain in $EuMnBi_2$ [9]. The expected cross-correlation response is intimately associated with a type of multipole, namely symmetry of the relevant ordered state. Thus, a proper description of the ordered state is essential for a full understanding of the cross-correlation phenomenon observed experimentally.

The uranium-based antiferromagnetic (AFM) compound UNi_4B has been intensively studied not only as a frustrated magnet but also as the first metallic compound exhibiting a current-induced M. [7] For a long time, the crystal structure of this compound was considered to be hexagonal with space group $P6/mmm$. [10, 11] In addition, below an AFM ordering temperature $T_N = 20.4$ K, it has been believed that two-thirds of the U moments form a vortexlike structure on a honeycomb network [11], which can be regarded as a ferroic MTD ordering with sixfold rotational symmetry. [6] This MTD ordering can explain the experimentally observed in-honeycomb plane M induced by an in-plane electric current. [6, 7] On the other hand, it fails to explain the in-plane M induced by an out-of-plane current, which was also experimentally observed. [12] Thus, further experimental examination of the AFM structure remains a crucial issue.

Furthermore, it has recently been confirmed that UNi_4B has an orthorhombic structure (space group $Cmcm$) with a lower symmetry than the hexagonal structure. [13–16] The a axis of the orthorhombic structure a_o corresponds to the c axis of the hexagonal structure c_h ($\parallel$ [0001]), b_o corresponds to b_h ($\parallel$ $[01\bar{1}0]$), and c_o corresponds to a_h ($\parallel$ $[2\bar{1}\bar{1}0]$). [13, 17] This lowering of crystal symmetry should influence the anisotropy of physical properties and the symmetry of the AFM structure, such as a tilted toroidal ordering [14]. It is worth noting that a new type of ordering with threefold rotational symmetry, named a triforce ordering, has recently been proposed to explain the out-of-plane current-induced M component by taking the orthorhombic distortion into account. [12]

To elucidate the AFM structure in UNi_4B, experimental verification based on the orthorhombic structure is essential, however, macroscopic measurements from this perspective are lacking. For example, magnetic field–temperature (H-T) phase diagrams obtained thus far have been constructed based on a hexagonal structure. [17, 18] The phase diagrams for $H \parallel a_h$ and b_h consist of multiple phases below T_N, whose boundaries are characterized by metamagnetic transitions, indicative of spin reorientation. [10, 18] In addition, the role of Γ_6-type electric quadrupoles in the H-induced transitions has also been pointed out. [17] The mechanism of H-induced transitions and their H angular dependences should be governed by the symmetry of the crystal and magnetic

* Contact author: hidaka@phys.sci.hokudai.ac.jp

structures; nevertheless, the details remain unclear.

In this study, we measured thermal expansion and magnetostriction under H using a single crystal of UNi_4B oriented based on the orthorhombic structure and constructed H–T phase diagrams within the b_oc_o plane. The insights into the H angular dependence of the H–T phase diagram and lattice distortions associated with the H-induced transitions will provide essential information for understanding the AFM ordered states of UNi_4B.

II. EXPERIMENTAL DETAILS

A single crystal of UNi_4B was grown by the Czochralski method using a tetra-arc furnace. The crystallographic axes of the orthorhombic structure in the measured sample were determined using an x-ray four-circle diffractometer.

Linear thermal expansion $\Delta L(T)/L$ and magnetostriction $\Delta L(H)/L$ measurements were performed using strain gauges (KFLB-02-120-C1-16 with resistance $R = 120\ \Omega$, Kyowa Electronic Instruments) by the two-gauge active dummy method (Kelvin double bridge method) to compensate the effects of temperature and magnetic field. [19] The active and dummy gauges were glued to the surface of the sample and a pure copper block, respectively, using gauge cement. The $\Delta L(H)/L$ data presented in this paper have been corrected by removing a linear time-dependent component. [20] In addition, magnetostriction of the copper block and a difference in magnetoresistance between the active and dummy gauges were not taken into account.

$\Delta L(T)/L$ and $\Delta L(H)/L$ were measured along the a_o axis in a temperature range of 2–300 K and in a magnetic field range up to 14 T using a physical property measurement system (PPMS; Quantum Design). The current applied to the circuit was $I = 100\ \mu$A. Under this applied current, the actual sample temperature below $\sim$4 K may be some hundred mK higher than the set temperature value due to the Joule heating of the strain gauges, e.g., 2.0 + 0.5 K at the lowest set temperature of 2 K. [20] A magnetic field H was applied within the b_oc_o plane. Here, we define θ as a H angle from the c_o axis within the b_oc_o plane.

III. RESULTS

A. $H \parallel c_o$ and b_o

Temperature dependence of the linear thermal expansion in UNi_4B along the a_o axis $[= \Delta L_a(T)/L_a]$ below 30 K at several fields for $H \parallel c_o$ ($\theta = 0°$) and $H \parallel b_o$ ($\theta = 90°$) are shown in Figs. 1(a) and 1(b), respectively. At zero field, a kink is observed at T_N, below which the lattice along a_o spontaneously shrinks. Below $\sim$ 12 K, the lattice begins to expand upon cooling. This expansion may be related to some remaining degrees of freedom in

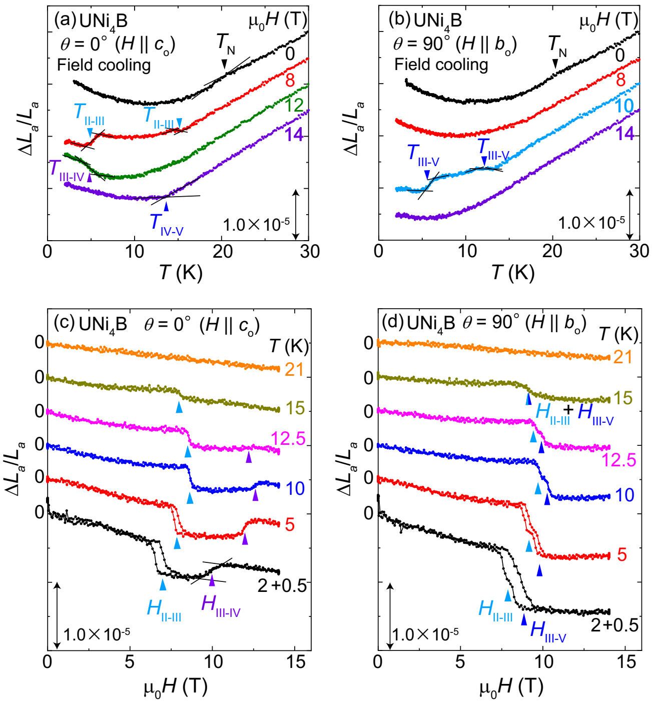

FIG. 1. (Color online) Thermal expansion $\Delta L_a(T)/L_a$ for (a) $H \parallel c_o$ and (b) $H \parallel b_o$ in UNi_4B at selected fields during the field-cooling (FC) process. Magnetostriction $\Delta L_a(H)/L_a$ for (c) $H \parallel c_o$ and (d) $H \parallel b_o$ at selected temperatures. In all the figures, the data are shifted vertically for ease of viewing.

the ordered state, as pointed out by previous specific heat [21], NMR [22], and ultrasound measurements [17]. Note that the thermal expansion coefficient obtained in this study shows close agreement above $\sim$10 K with the previous study [21], although the present data show larger negative values below $\sim$10 K compared to the previous data (shown in Supplemental Material [20]).

Figure 1(c) shows the magnetostriction along the a_o axis $[= \Delta L_a(H)/L_a]$ up to 14 T at several fixed temperatures for $H \parallel c_o$. In this paper, the transition point between two ordered phases is termed, for example, as $H_{\mathrm{II-III}}$ between phases II and III. The $\Delta L_a(H)/L_a$ curve measured at 2 K shows a notable decrease with hysteresis at a transition field $H_{\mathrm{II-III}}$, followed by an increase without (or with negligibly small) hysteresis at $H_{\mathrm{III-IV}}$. This behavior persists up to 12.5 K, but at 15 K, the increase at $H_{\mathrm{III-IV}}$ disappears. The $\Delta L_a(T)/L_a$ curves at 8 and 12 T also show corresponding anomalies at $T_{\mathrm{II-III}}$ and $T_{\mathrm{III-IV}}$, respectively, as shown in Fig. 1(a). In addition, a $T_{\mathrm{IV-V}}$ transition can be observed in $\Delta L_a(T)/L_a$ at 13 and 14 T, which can be distinguished from T_N determined from a previous study. [17]

For $H \parallel b_o$, the $\Delta L_a(H)/L_a$ curves show two successive transitions at $H_{\mathrm{II-III}}$ and $H_{\mathrm{III-V}}$ that are nearly degenerated. This slight splitting of these transition fields has not been reported in previous studies, [17, 18] and it is difficult to determine whether it is intrinsic in nature or arises from the experimental misalignment of θ in this

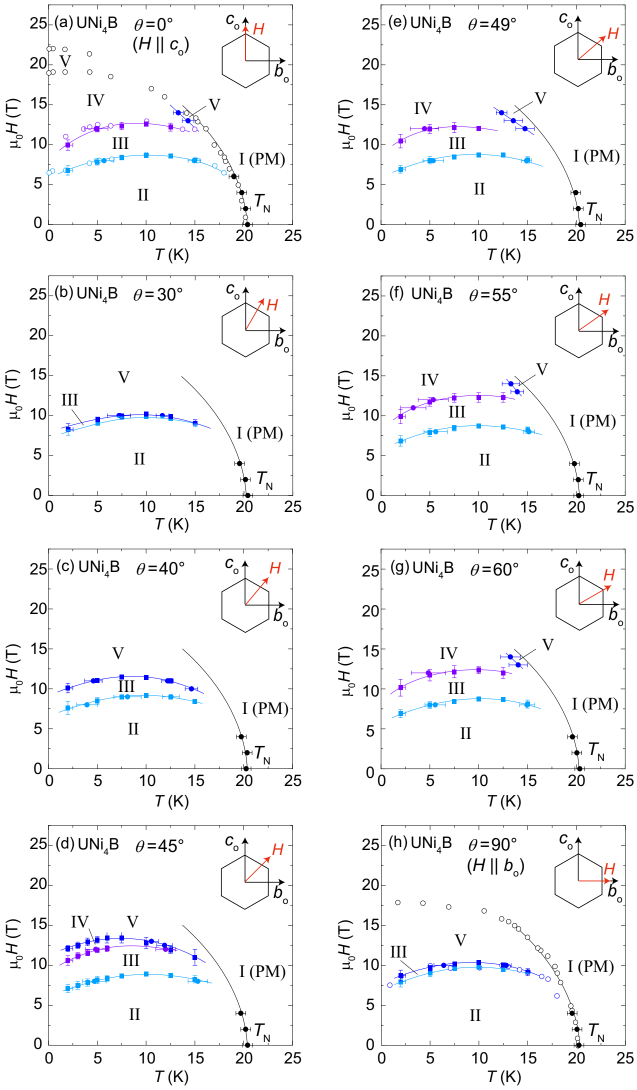

FIG. 2. (Color online) H-T phase diagrams of UNi4B constructed from $\Delta L_a(T)/L_a$ (solid circles) and $\Delta L_a(H)/L_a$ (solid squares) for (a) $\theta = 0°$ (parallel to the orthorhombic $c_{\rm o}$ axis), (b) 30°, (c) 40°, (d) 45°, (e) 49°, (f) 55°, (g) 60°, and (h) 90° (parallel to the orthorhombic $b_{\rm o}$ axis). In (a) and (h), the data obtained from the previous ultrasound measurements are also plotted for comparison (open circles). [17] Here, we plotted their data by swapping the hexagonal $a_{\rm h}$ and $b_{\rm h}$ axes. In (b)–(g), the black solid curves represent $T_{\rm N}$ determined from previous ultrasound measurements. [17] All the solid curves are guides for the eye.

study. In addition, it is significant that $\Delta L_a(H)/L_a$ decreases at $H_{\rm III-V}$ accompanied by hysteresis, unlike the increase without hysteresis observed at $H_{\rm III-IV}$ for $H \parallel c_{\rm o}$. The anomalies at $T_{\rm III-V}$ can be also observed in the $\Delta L_a(T)/L_a$ curve at 10 T [see Figs. 1(b)].

The H-T phase diagrams for $H \parallel c_{\rm o}$ and $b_{\rm o}$ constructed in this study are shown in Figs. 2(a) and 2(h), respectively. Here, the transition points determined from $\Delta L_a(T)/L_a$ were estimated based on data obtained from the cooling and heating processes. [20] In these figures, the transition points determined from ultrasound measurements are also plotted (open circles), although their study has been done based on a hexagonal structure. [17] Here, it should be noted that we plotted their data by swapping the $a_{\rm h}$ and $b_{\rm h}$ axes. [20] It is evident that the present results are identical to the previously reported phase diagrams by Mentink et al. [18] and Yanagisawa et al. [17]

B. Intermediate angle

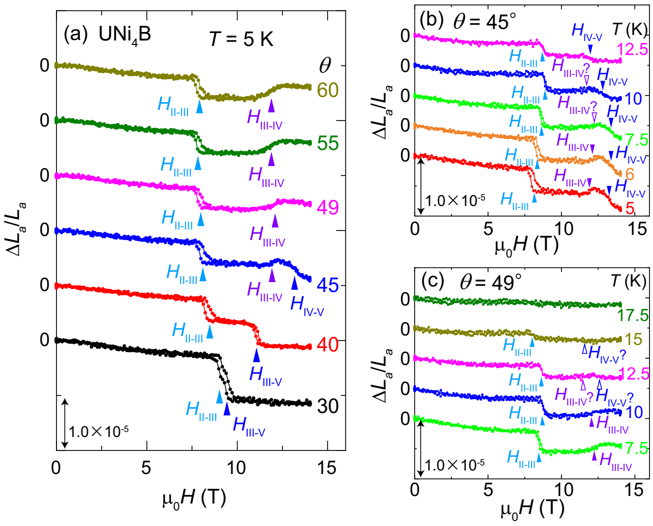

FIG. 3. (Color online) (a) $\Delta L_a(H)/L_a$ at 5 K between $\theta = 30°$ and 60°. $\Delta L_a(H)/L_a$ for (b) $\theta = 45°$ between 5 and 12.5 K and (c) $\theta = 49°$ between 7.5 and 17.5 K. The open triangles represent possible transition points (not plotted in the phase diagrams of Fig. 2). The data are shifted vertically for ease of viewing in these figures.

Figure 3(a) shows $\Delta L_a(H)/L_a$ of UNi4B at 5 K between $\theta = 30°$ and 60°. The data for $\theta = 30°$ and 60° are quite similar to those for 90° and 0°, respectively, except for a slight difference in the splitting width of the nearly degenerate H-induced transitions between 30° and 90°. The split of $H_{\rm II-III}$ and $H_{\rm III-V}$ becomes larger with increasing θ from 30°. It is noteworthy that, at 45°, a tiny increase in $\Delta L_a(H)/L_a$ can be observed just before the second decrease. This indicates that three successive transitions occur at this angle, named $H_{\rm II-III}$, $H_{\rm III-IV}$, and $H_{\rm IV-V}$. In the $\Delta L_a(H)/L_a$ curves above 49° (= the [011] direction), the second decrease disappears, but the increase at $H_{\rm III-IV}$ becomes clearly observable instead. Furthermore, we show how the $H_{\rm III-IV}$ and $H_{\rm IV-V}$ transitions evolve as a function of temperature on the $\Delta L_a(H)/L_a$ data for 45° and 49° in Figs. 3(b) and 3(c), respectively.

Figures 2(b)–(g) show the H-T phase diagrams for θ's of 30°, 40°, 45°, 49°, 55°, and 60°, respectively. The black solid curves represent the phase boundary of

T_N determined from previous ultrasound measurements. [17] Here, the phase boundaries of T_N show no clear H-direction dependence between a_h and b_h below $\sim$ 15 T. [17] One can see a small region of phase IV at 45°, and it expands into the high-H region with increasing θ.

C. Magnetic field angle phase diagram

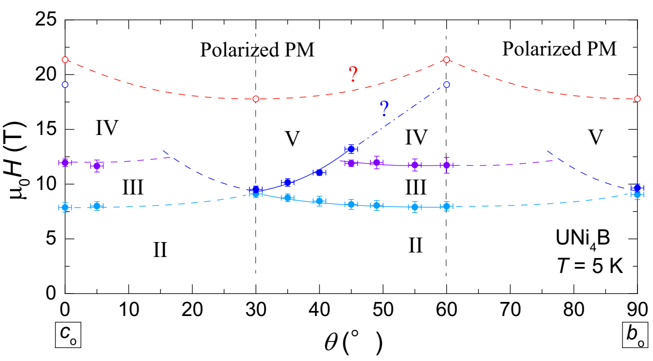

FIG. 4. (Color online) Magnetic field angle magnetic phase diagram of UNi4B at 5 K. The open circles are H_{IV-V} and H_N determined at 4.2 K from a previous ultrasound study. [17] The solid and dashed-dotted curves are guides to the eye, and the dashed curves represent phase boundaries, assuming sixfold rotational symmetry.

Figure 4 shows the H-θ magnetic phase diagram at 5 K in the θ range between 0° and 90°. The open symbols are H_{IV-V} and H_N determined at 4.2 K by Yanagisawa et al., although their ultrasound study has been performed based on the hexagonal structure. [17] The dashed curves represent the phase boundaries, assuming a sixfold symmetry. Mentink et al. reported that the H_{II-III} transition shows sixfold symmetry. [18] It is intriguing that the split between H_{II-III} and H_{III-V} does not become simply larger toward 60°, instead, phase IV is inserted between III and V above 45°. This result may explain the presence of H_{IV-V} for a_h (= b_h in the original paper [17]) and the absence for b_h (= a_h in Ref. [17]) suggested by Yanagisawa et al., [17, 20] as indicated by the dashed-dotted curve in Fig. 4. Further measurements under higher H for the intermediate angles are necessary.

IV. DISCUSSION

We discuss the possible origin of the observed lattice distortions associated with the phase transitions in UNi_4B. Two important mechanisms are known to be involved in magnetostriction in $4f$-electron systems: the crystalline-electric-field (CEF) model and exchange striction model. [23] The lattice along the a_o axis spontaneously shrinks below T_N at zero field, while the lattice perpendicular to a_o expands. [21] On the other hand, the magnetic ordered moments lie within the b_oc_o plane below T_N [11, 14], which should be attributed to the magnetic anisotropy due to the CEF effect. [17, 24, 25] From these in-plane moments, naively, it is expected that the $5f$ orbital has a larger distribution along the a_o axis. If layers containing Ni ions, which sandwich an atomic layer containing U ions, are positively charged [13], the Ni layers are attracted to the $5f$ orbital by a Coulomb attraction below T_N, resulting in a spontaneous lattice contraction along a_o.

The present magnetostriction measurements also indicate the lattice contractions along a_o accompanying the H-induced transitions in the AFM ordered state, except for the expansion at H_{III-IV}. Since the H-induced transitions are considered to originate from the spin flop within the b_oc_o plane [18], these lattice contractions may be dominated by the intersite exchange interactions between the magnetic moments (the exchange striction model) rather than the single-site effect (the CEF model). [23] The exchange interaction in this system should depend on the distance between the U ions through the Ruderman-Kittel-Kasuya-Yosida interaction. The U-U distance within the plane may increase by the spin flop until the distance where the ferromagnetic interaction becomes stable, resulting in a lattice contraction along the a_o axis. In $ErGa_2$, such an exchange-striction model has been applied to similar magnetostrictions associated with the spin flop. [26]

On the other hand, the same exchange striction model appears to have difficulty in explaining the lattice expansion at H_{III-IV}, because $M(H)$ shows a steep increase even at this transition field. [18] If the ordered moments are tilted toward the a_o direction, the distribution of the $5f$ orbitals along the a_o axis decreases. As a result, the lattice along a_o may expand. However, it is uncertain whether such a tilt occurs when H is applied within the plane. To understand the origin of the nonmonotonic magnetostrictions associated with the H-induced transitions, contributions of the electric quadrupoles and one-third of U magnetic moments, which remain disordered below T_N, should also be taken into account.

Finally, we comment on the rotational symmetry of the AFM structure within the b_oc_o plane in UNi_4B. This study revealed that the H-T phase diagrams of UNi_4B for θ of 0° and 60° are identical within experimental accuracy, as can be seen in Fig. 2. On the other hand, the phase diagrams for 30° and 90° are also identical, except for the slight difference in the splitting width of the nearly degenerate H-induced transitions, which may be due to the experimental misalignment of θ ($\sim \pm$ 1°). Thus, we argue that the H-T phase diagram of UNi_4B practically exhibits sixfold rotational symmetry within the b_oc_o plane, although twofold rotational symmetry is generally expected under an orthorhombic structure. This fact suggests that the effect of orthorhombic distortion on the rotational symmetry of the H-T phase diagram is too small to be detected, at least within present experimental accuracy, and the observed effective sixfold rotational symmetry is plausibly attributed to a quasihexagonal structure formed by U ions.

Note that the present result does not necessarily mean that the magnetic structure also exhibits sixfold rotational symmetry. The most straightforward interpretation of the AFM structure in UNi_4B is a toroidal magnetic ordering with sixfold rotational symmetry or a slightly distorted toroidal ordering with twofold rotational symmetry. [6, 14] On the other hand, a triforce ordering with threefold rotational symmetry or a slightly distorted triforce ordering may also explain the observed effective sixfold rotational symmetry of the magnetic phase diagram if the ordered state contains multiple domains. [12] To elucidate the rotational symmetry of the AFM states in UNi_4B, further experimental investigations of various physical quantities, such as electrical transport and M, along with theoretical calculations, are required.

V. SUMMARY

We have investigated lattice distortions along the a_o axis associated with H-induced transitions in an AFM state of UNi_4B and constructed H-T phase diagrams for H's applied within the b_oc_o plane. The H-T phase diagrams for θ of 0° (= c_o) and 90° (= b_o) are identical to those for 60° and 30° within experimental accuracy, respectively, except for a slight difference in the splitting width of successive H-induced transitions between θ = 30° and 90°. This fact suggests that the H-T phase diagram of UNi_4B practically exhibits sixfold rotational symmetry within the b_oc_o plane. In addition, the splitting of nearly degenerate H-induced transitions observed at $\theta = 30°$ does not become simply larger toward 60° with increasing θ; a unique phase IV characterized by lattice expansion is inserted between III and V above 45°. The insights obtained from this study will guide us to a full understanding of current-induced M found in UNi_4B through the proper description of the AFM structure.

ACKNOWLEDGMENTS

The authors are grateful to S. Onodera and R. Murata for their experimental support and to H. Saito, H. Kusunose, S. Hayami, and T. Ishitobi for their helpful comments. Crystal orientation was determined using an offline x-ray four-circle diffractometer at the High Energy Accelerator Research Organization (KEK), with technical support provided by H. Nakao. The present research was supported by JSPS KAKENHI Grants No. JP23H04867, No. JP23H04868, No. JP23H04870, No. JP23K25810, and No. JP23K03294, and the Toyota Riken Scholar Program. This study was also partly supported by Hokkaido University, Global Facility Center (GFC), Advanced Physical Property Open Unit (APPOU), funded by MEXT under the "Support Program for Implementation of New Equipment Sharing System," Grant No. JPMXS0420100318.

DATA AVAILABILITY

The data that support the findings of this article are not publicly available. The data are available from the authors upon reasonable request.

[1] D. N. Astrov, The magnetoelectric effect in antiferromagnetics, Sov. Phys. JETP **11**, 708 (1960).

[2] V. J. Folen, G. T. Rado, and E. W. Stalder, Anisotropy of the magnetoelectric effect in Cr_2O_3, Phys. Rev. Lett. **6**, 607 (1961).

[3] S. Hayami, M. Yatsushiro, Y. Yanagi, and H. Kusunose, Classification of atomic-scale multipoles under crystallographic point groups and application to linear response tensors, Phys. Rev. B **98**, 165110 (2018).

[4] S. Hayami and H. Kusunose, Microscopic description of electric and magnetic toroidal multipoles in hybrid orbitals, J. Phys. Soc. Jpn. **87**, 033709 (2018).

[5] H. Watanabe and Y. Yanase, Group-theoretical classification of multipole order: Emergent responses and candidate materials, Phys. Rev. B **98**, 245129 (2018).

[6] S. Hayami, H. Kusunose, and Y. Motome, Toroidal order in metals without local inversion symmetry, Phys. Rev. B **90**, 024432 (2014).

[7] H. Saito, K. Uenishi, N. Miura, C. Tabata, H. Hidaka, T. Yanagisawa, and H. Amitsuka, Evidence of a new current-induced magnetoelectric effect in a toroidal magnetic ordered state of UNi_4B, J. Phys. Soc. Jpn. **87**, 033702 (2018).

[8] M. Shinozaki, G. Motoyama, M. Tsubouchi, M. Sezaki, J. Gouchi, S. Nishigori, T. Mutou, A. Yamaguchi, K. Fujiwara, K. Miyoshi, and Y. Uwatoko, Magnetoelectric effect in the antiferromagnetic ordered state of Ce_3TiBi_5 with Ce zig-zag chains, J. Phys. Soc. Jpn. **89**, 033703 (2020).

[9] Y. Shiomi, H. Masuda, H. Takahashi, and S. Ishiakwa, Large magneto-piezoelectric effect in $EuMnBi_2$ single crystal at low temperatures, Scientific Reports, **10**, 7574 (2020).

[10] S. Mentink, H. Nakotte, A. de Visser, A. Menovsky, G. Nieuwenhuys, and J. Mydosh, Reduced-moment antiferromagnetism in single-crystal UNi_4B, Physica B **186–188**, 270 (1993).

[11] S. A. M. Mentink, A. Drost, G. J. Nieuwenhuys, E. Frikkee, A. A. Menovsky, and J. A. Mydosh, Magnetic ordering and frustration in hexagonal UNi_4B, Phys. Rev. Lett. **73**, 1031 (1994).

[12] T. Ishitobi and K. Hattori, Triple-Q partial magnetic orders induced by quadrupolar interactions: Triforce order scenario for UNi_4B, Phys. Rev. B **107**, 104413 (2023).

[13] C. Tabata, H. Sagayama, H. Saito, H. Nakao, and H. Amitsuka, X-ray crystal structure analysis of magnetoelectric metal UNi_4B, J. Phys. Soc. Jpn. **90**, 064601 (2021).

[14] J. Willwater, S. Süllow, M. Reehuis, R. Feyerherm, H. Amitsuka, B. Ouladdiaf, E. Suard, M. Klicpera, M. Vališka, J. Pospíšil, and V. Sechovský, Crystallographic and magnetic structure of $UNi_4{}^{11}B$, Phys. Rev. B **103**, 184426 (2021).

[15] R. Takeuchi, Y. Kishimoto, H. Kotegawa, H. Harima, Y. Homma, F. Honda, A. Nakamura, Y. Shimizu, D. X. Li, D, Aoki, and H. Tou, ^{11}B-NMR investigation for crystal structure in antiferromagnet UNi_4B, JPS Conf. Proc. **29**, 013001 (2020).

[16] Y. Haga, A. Oyamada, T. Matsuda, S. Ikeda, and Y. Ōunki, Crystal structure of frustrated antiferromagnet UNi_4B, Physica B **403**, 900 (2008).

[17] T. Yanagisawa, H. Matsumori, H. Saito, H. Hidaka, H. Amitsuka, S. Nakamura, S. Awaji, D. I. Gorbunov, S. Zherlitsyn, J. Wosnitza, K. Uhlířová, M. Vališka, and V. Sechovský, Electric quadrupolar contributions in the magnetic phases of UNi_4B, Phys. Rev. Lett. **126**, 157201 (2021).

[18] S. A. M. Mentink, G. J. Nieuwenhuys, H. Nakotte, A. A. Menovsky, A. Drost, E. Frikkee, and J. A. Mydosh, Magnetization and resistivity of UNi_4B in high magnetic fields, Phys. Rev. B **51**, 11567 (1995).

[19] N. Kabeya, K. Imura, K. Deguchi, and N. K. Sato, Thermal expansion measurements using the strain gauge technique with Kelvin double bridge, J. Phys. Soc. Jpn. **80**, SA098 (2011).

[20] See Supplemental Materials for (1) correction of linear time dependence in magnetostriction, (2) influence of Joule heating induced by applied current, (3) thermal expansion coefficient at zero magnetic field, (4) $\Delta L_a(T)/L_a$ on cooling and heating processes, and (5) comparison of previously reported H-T phase diagrams.

[21] S. Mentink, H. Amitsuka, A. de Visser, Z. Slanič, D. P. Belanger, J. J. Neumeier, J. D. Thompson, A. A. Menovsky, J.A. Mydosh, and T. E. Mason, Thermodynamic study of the magnetic phase transition in UNi_4B, Physica B **230–232**, 108 (1997).

[22] A. Oyamada, M. Kondo, F. Fukuoka, T. Itou, S. Maekawa, D.X. Li, and Y. Haga, NMR studies of the partially disordered state in a triangular antiferromagnet UNi_4B, J. Phys.: Condens. Matter. **19**, 145246 (2007).

[23] M. Doerr, M. Rotter, and A. Lindbaum, Magnetostriction in rare-earth based antiferromagnets, Adv. Phys. **54**, 1 (2005).

[24] A. S. Ermolenko, Magnetocrystalline anisotropy of rare earth intermetallics, IEEE Trans. Magn. **12**, 992 (1976).

[25] R. Skomski and D.J. Sellmyer, Anisotropy of rare-earth magnets, J. Rare Earths **27**, 675 (2009).

[26] P. E. Markin and N. V. Baranov, Phys. Metals Metallog. **85**, 158 (1998), as cited in Ref. [23].